

Molecular detection of maturation stages in the developing kidney

長沼, 英和

<https://hdl.handle.net/2324/4495962>

出版情報 : Kyushu University, 2021, 博士 (医学) , 課程博士
バージョン :
権利関係 :





Molecular detection of maturation stages in the developing kidney

Hidekazu Naganuma^{a,b,2}, Koichiro Miike^{a,2}, Tomoko Ohmori^a, Shunsuke Tanigawa^a, Takumi Ichikawa^{c,1}, Mariko Yamane^{c,1}, Masatoshi Eto^b, Hitoshi Niwa^c, Akio Kobayashi^a, Ryuichi Nishinakamura^{a,*}

^a Department of Kidney Development, Institute of Molecular Embryology and Genetics, Kumamoto University, 2-2-1 Honjo, Chuo-ku, Kumamoto 860-0811, Japan

^b Department of Urology, Kyushu University Graduate School of Medical Science, 3-3-1 Maidashi, Higashi-ku, Fukuoka 812-8582, Japan

^c Department of Pluripotent Stem Cell Biology, Institute of Molecular Embryology and Genetics, Kumamoto University, 2-2-1 Honjo, Chuo-ku, Kumamoto 860-0811, Japan

ARTICLE INFO

Keywords:

Kidney development
Single-cell RNA sequencing
Maturation
In situ hybridization

ABSTRACT

Recent advances in stem cell biology have enabled the generation of kidney organoids *in vitro*, and further maturation of these organoids is observed after experimental transplantation. However, the current organoids remain immature and their precise maturation stages are difficult to determine because of limited information on developmental stage-dependent gene expressions in the kidney *in vivo*. To establish relevant molecular coordinates, we performed single-cell RNA sequencing (scRNA-seq) on developing kidneys at different stages in the mouse. By selecting genes that exhibited upregulation at birth compared with embryonic day 15.5 as well as cell lineage-specific expression, we generated gene lists correlated with developmental stages in individual cell lineages. Application of these lists to transplanted embryonic kidneys revealed that most cell types, other than the collecting ducts, exhibited similar maturation to kidneys at the neonatal stage *in vivo*, revealing non-synchronous maturation across the cell lineages. Thus, our scRNA-seq data can serve as useful molecular coordinates to assess the maturation of developing kidneys and eventually of kidney organoids.

1. Introduction

The kidney is derived from at least two types of precursors: nephron progenitors and ureteric bud (Costantini and Kopan, 2010). The nephron progenitors give rise to nephrons including glomerular podocytes, proximal tubules, loops of Henle (LOH), and distal tubules, while the ureteric bud branches extensively to form the collecting ducts and ureter (Kobayashi et al., 2008) (Marose et al., 2008). These differentiated components align to form the route for urinary flow. The nephron progenitors and ureteric bud initiate their interactions around embryonic day (E) 11.5 in mice. At E15.5, the overall nephron segments are specified, but new nephrons continue to be generated from the nephron progenitors. After glomerular vascularization, urine starts to flow at E16.5–E17.5 (Rasouly and Lu, 2013). Meanwhile, the inner (medullary) region of the kidney elongates, reflecting elongation of the LOH and collecting ducts. This medullary region development continues after the day of birth (P0), while nephron progenitors cease self-renewal and disappear within a few days after birth (Hartman et al., 2007) (Rumballe et al., 2011) (Volovelsky et al., 2018).

Recent advances in stem cell biology have enabled the generation of kidney organoids *in vitro* (Morizane et al., 2015; Taguchi et al., 2014; Takasato et al., 2015). We previously created kidney organoids from pluripotent stem cells: mouse embryonic stem cells (ESCs) and human induced pluripotent stem cells (iPSCs) (Taguchi et al., 2014). However, it is becoming clear that the organoids *in vitro* remain at immature stages, equivalent to kidneys at approximately E14.5–E15.5 in mice and 10–14 weeks of gestation in humans (Taguchi and Nishinakamura, 2017; Takasato et al., 2015; Wu et al., 2018). We and others also developed methods to experimentally transplant kidney organoids into immunodeficient mice, allowing organoid vascularization and connection to the host circulation (Bantounas et al., 2018; Sharmin et al., 2016; Subramanian et al., 2019; Tanigawa et al., 2018; van den Berg et al., 2018). Upon transplantation, glomerular podocytes within the organoids acquire more mature morphological features related to the filtration function, possibly caused by an oxygen supply and/or interaction with vascular endothelial cells. While the precise mechanisms remain unsolved, transplantation is frequently utilized to induce maturation of organoids in the research field of stem cell biology.

* Corresponding author.

E-mail address: ryuichi@kumamoto-u.ac.jp (R. Nishinakamura).

¹ Present address: Laboratory for Bioinformatics Research, RIKEN Center for Biosystems Dynamics Research, Kobe 650-0047, Japan.

² Equal contribution.

Despite these advances, precise determination of maturation stages is difficult because of the lack of molecular coordinates i.e. comprehensive information on stage-dependent gene expressions in the developing kidney. Currently, these coordinates are not even available for mouse embryonic kidneys *in vivo*. This situation largely arises because of the increasing numbers of cell types during kidney development, with each cell type

containing small amounts of cells. Conventional gene expression analyses, which require large numbers of homogeneous cells, are not suitable for heterogeneous maturing kidneys. The GUDMAP database (www.gudmap.org) has accumulated large numbers of gene expression analyses in the developing kidney, including some in total kidneys and some in sorted or microdissected cells (McMahon et al., 2008). However, even the

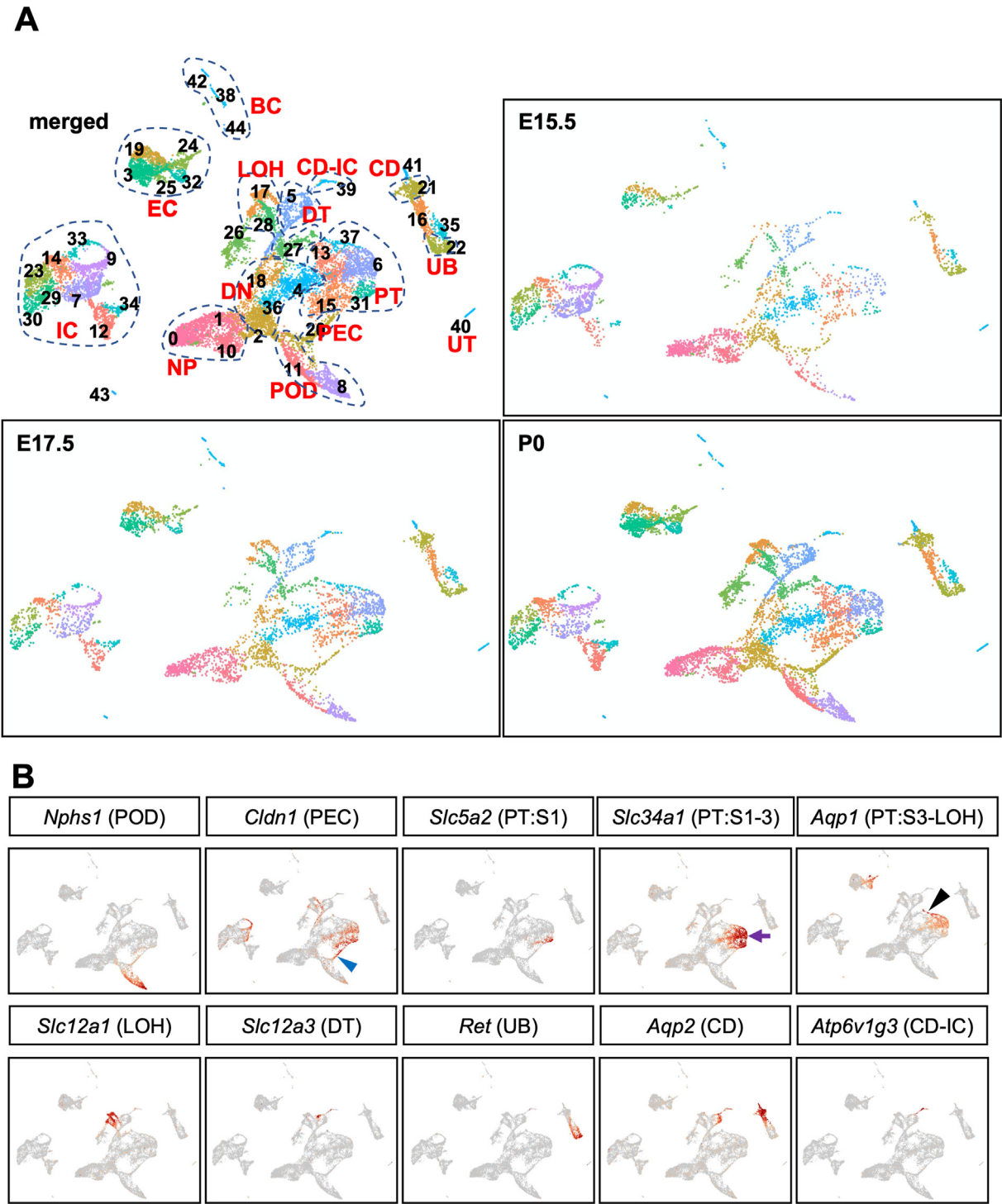


Fig. 1. Single-cell RNA-seq analysis of developing kidneys. (A) Merged and stage-specific UMAP plots of E15.5, 17.5, and P0 kidneys. NP: nephron progenitor; POD: podocyte; PEC: glomerular parietal epithelial cell; DN: differentiating nephron; PT: proximal tubule; LOH: loop of Henle; DT: distal tubule; UB: ureteric bud tip; CD: collecting duct; CD-IC: intercalated cell of collecting duct; IC: interstitial cell; EC: endothelial cell; UT: ureter; BC: blood cell. (B) Expressions of representative marker genes for nephrons and collecting duct segments in UMAP plots. Note that *Slc34a1* is expressed in all three segments of proximal tubules, although its expression in the S3 segment is weaker. *Aqp1* is expressed in the S3 segment of proximal tubules and descending limb of LOH (black arrowhead), as well as in endothelial cells. *Aqp2* is expressed in the collecting duct stalks and distal tubules. Blue arrowhead: PEC; purple arrow: S2 segment.

latter analyses often contain cells from multiple stages, and thus the data are not directly useable for maturation analyses.

Single-cell RNA sequencing (scRNA-seq) analysis has enabled the examination of gene expressions in complicated and heterogeneous organs, including the kidney, and some of these data have been deposited in the GUDMAP database (Adam et al., 2017a; Combes et al., 2019a, 2019b; Lindström et al., 2018; Magella et al., 2017; Ransick et al., 2019; Wang et al., 2018; Wu et al., 2018). However, most of these previous studies analyzed embryonic or adult kidneys at a single time point, or compared *in vivo* kidneys with *in vitro* kidney organoids. Thus, few studies have addressed kidney maturation from mid-gestation to birth for a limited cell type (Chen et al., 2015). To establish molecular coordinates for kidney maturation in the present study, we performed scRNA-seq on developing mouse kidneys at different stages, and selected maturation-dependent genes. We further assessed the maturation status of transplanted embryonic kidneys by comparing the RNA-seq data and expressions of maturation-dependent genes. Our RNA-seq data and the selected gene lists will serve as reference tools for maturation of developing kidneys and eventually of kidney organoids.

2. Results

2.1. scRNA-seq analysis of developing kidneys

We performed scRNA-seq on developing mouse kidneys at three different stages: E15.5, E17.5, and P0. High-quality data were obtained, with medium reads of 4,493, 2,360, and 2467 genes per cell, respectively. After analysis of the data using Seurat v3.1.1 (Butler et al., 2018; Stuart et al., 2019a), the cells were classified into 45 clusters, with a larger number of solid clusters at P0 than at E15.5 (Fig. 1A). We identified cell types for most of the clusters using cell type-specific markers: nephron progenitors (*Six2*+, clusters 0, 1, and 10), glomerular podocytes (*Nphs1*+, clusters 8 and 11), glomerular parietal epithelial cells (*Claudin 1* (*Cldn1*)+, cluster 20), proximal tubules (S1 segment: *Solute carrier family 5a2* (*Slc 5a2*)+, clusters 15 and 31; S2 segment: *Slc5a2*–/*Slc34a1*+, clusters 13 and 6; S3 segment: *Aquaporin 1* (*Aqp1*)+/ *Slc7a13*+ (Lee et al., 2015; Ransick et al., 2019), cluster 37), LOH (thin descending limb: *Aqp1*+/ *Slc39a8*+ (Lee et al., 2015; Ransick et al., 2019), cluster 27; thick ascending limb: *Uromodulin* (*Umod*)+/ *Slc12a1*+, clusters 28 and 17), distal tubules (*Slc12a3*+, cluster 5), ureteric bud tips (*Ret*+, clusters 22 and 35), and collecting duct stalks (*Aqp2*+, clusters 16, 21, and 41) (Fig. 1B, Fig. S1A). Intercalated cells formed a cluster that was separated from the collecting duct clusters (*Atp6v1g3*+, cluster 39) (Fig. 1B). Interstitial cells were classified into multiple clusters (7, 9, 12, 14, 23, 29, 30, 33, and 34), among which clusters 9/33, 12, and 34 may represent stromal progenitors (*Foxd1*+ (Kobayashi et al., 2014)), mesangial cells (*Nt5e*+, and renin-producing cells (*Ren1*+) , respectively (Fig. S1B). Endothelial cell clusters (*Pecam1*+, clusters 3, 19, 24, 25, and 32) contained *Ehd3*+ cells (cluster 32, Fig. S1C), which likely represented glomerular endothelial cells (Patrakka et al., 2007). Thus, Seurat v3.1.1, which utilizes integration anchors to cluster nearest neighbors (Stuart et al., 2019b), successfully categorized numerous cell types in the kidneys at different developmental stages.

2.2. Temporal changes in transcription factor expressions and developmental signaling activities during kidney maturation

Nephron progenitors were classified into three clusters (Fig. S1D): cluster 0 containing *Six2*+/ *Cited1*+ naïve cells, cluster 10 containing *Six2*+/ *Cited1*+/ *Top2a* + proliferating naïve cells, and cluster 1 containing *Six2*+/ *Cited1*–/ *Wnt4*+ primed cells (Boyle et al., 2008; Kobayashi et al., 2008; Self et al., 2006). During nephron segment specification, the nephron progenitor population first formed a *Mafb* + podocyte branch, which eventually differentiated into *Nphs1*+ podocytes (Figs. 1B and 2A). The branches for proximal tubules and LOH/distal tubules formed separately from the podocyte branch. Precursor cells for proximal tubules

expressed the transcription factor genes *Osr2* and then *Hnf4a* (Fig. 2B), the latter of which regulates maturation-dependent genes in proximal tubules (Deacon et al., 2019; Marable et al., 2018, 2020; Martovetsky et al., 2013). Common precursor cells for LOH/distal tubules expressed both *Pou3f3* (Nakai et al., 2003) and *Sim1*, with subsequent expression of *Sim2* and *Gata3* after specification of LOH and distal tubules, respectively (Fig. 2C). *Tfp2b*, recently reported to be important for distal nephron development (Marneros, 2020), was also detected in LOH and distal tubules (Fig. S1E). Thus, temporal shifts in transcription factor expressions occur in individual nephron segments during kidney maturation, and the clusters at the peripheral ends of the branches (clusters 5, 6, 8, 17, 31, and 37) represent the most mature stage in each lineage.

From the viewpoint of developmental signals, an indicator for WNT signaling pathway activity, *Axin2*, was mainly detected in developing distal tubules, as previously reported (Jho et al., 2002). *Fgf8* and *Etv4*, an indicator for FGF signaling activity (Mao et al., 2009), were also expressed in developing distal tubules, but restricted to an immature stage. In contrast, *Bmp7* (Oxburgh et al., 2005) was expressed in distal tubules at both immature and mature stages as well as in podocytes, while *Bmp4* (Miyazaki et al., 2000) was mainly detected in proximal tubules. We also noted that the activities of the major signaling pathways were downregulated in mature cells in most nephron segments. For example, *Axin2* (WNT signaling indicator) and *Etv4* (FGF signaling indicator) were absent in mature podocytes, and proximal and distal tubules (Fig. 2D). The same tendency was observed for *Hey1* (Notch signaling indicator), while *Hes1* was only downregulated in podocytes and proximal tubules (Fig. 2E). A BMP signaling indicator, *Id1* (Korchynskiy and Ten Dijke, 2002; López-Rovira et al., 2002), was decreased in mature podocytes and distal tubules (Fig. 2F). Thus, nephron segment-specific developmental signaling activation, followed by downregulation, is observed during kidney maturation.

2.3. Developmental stage-dependent gene lists for individual cell lineages

Our scRNA-seq analysis showed that UMAP clusters expressing some established lineage-restricted differentiation markers were already present at E15.5 (Fig. 1B). To identify stage-dependent genes for individual nephron segments, we first compared the gene expressions between E15.5 and P0 in the most mature clusters of each lineage, and picked up genes that were significantly upregulated or downregulated at P0 compared with E15.5. However, we found that these lists included genes associated with cellular stress, such as heat shock protein genes, *Jun/Fos* family genes, and *Gadd45* genes (Adam et al., 2017a), which may be evoked by the harsher cell dissociation processes used for P0 kidneys. Because these genes were ubiquitously expressed, it was difficult to discriminate them from maturation-dependent genes that were ubiquitously expressed. Thus, we decided to select cell-type specific genes and picked up the upregulated or downregulated genes in the corresponding clusters between the two stages. Most of the upregulated genes at P0 showed consistent results in UMAP plots, while the downregulated genes showed less prominent differences between the two stages. In addition, the downregulated genes were detected in more immature cell clusters at P0, reflecting the repetitive differentiation processes from nephron progenitors. Therefore, we decided to focus on the upregulated genes (fold change, >2.5), and curated each candidate gene for its spatiotemporal expression based on the UMAP plots. Violin plots of the finally selected genes showed their stage-dependent expressions in individual cell lineages (Fig. 3A, Figs. S2, S3, S4A, Table S1). Dot plots confirmed their cell type-specific expressions (Fig. 3B), although many genes selected for the S2 segment of proximal tubules were also expressed in the S1 and S3 segments. These selected gene lists included *Collagen type 4 alpha3 chain* (*Col4a3*) and *Semaphorin 3g* for podocytes, *Slc5a12* (lactate transporter) and *Cytochrome P450 family 27b1* (alpha hydroxylase of vitamin D) for proximal tubules, *Umod* and *Prostaglandin E receptor 3* (*Ptger3*) for LOH, *Aqp2* and *Aqp3* for collecting ducts, and *Lipocalin 2* (*Lcn2*) for ureteric bud tips. Most of the genes were already upregulated at E17.5

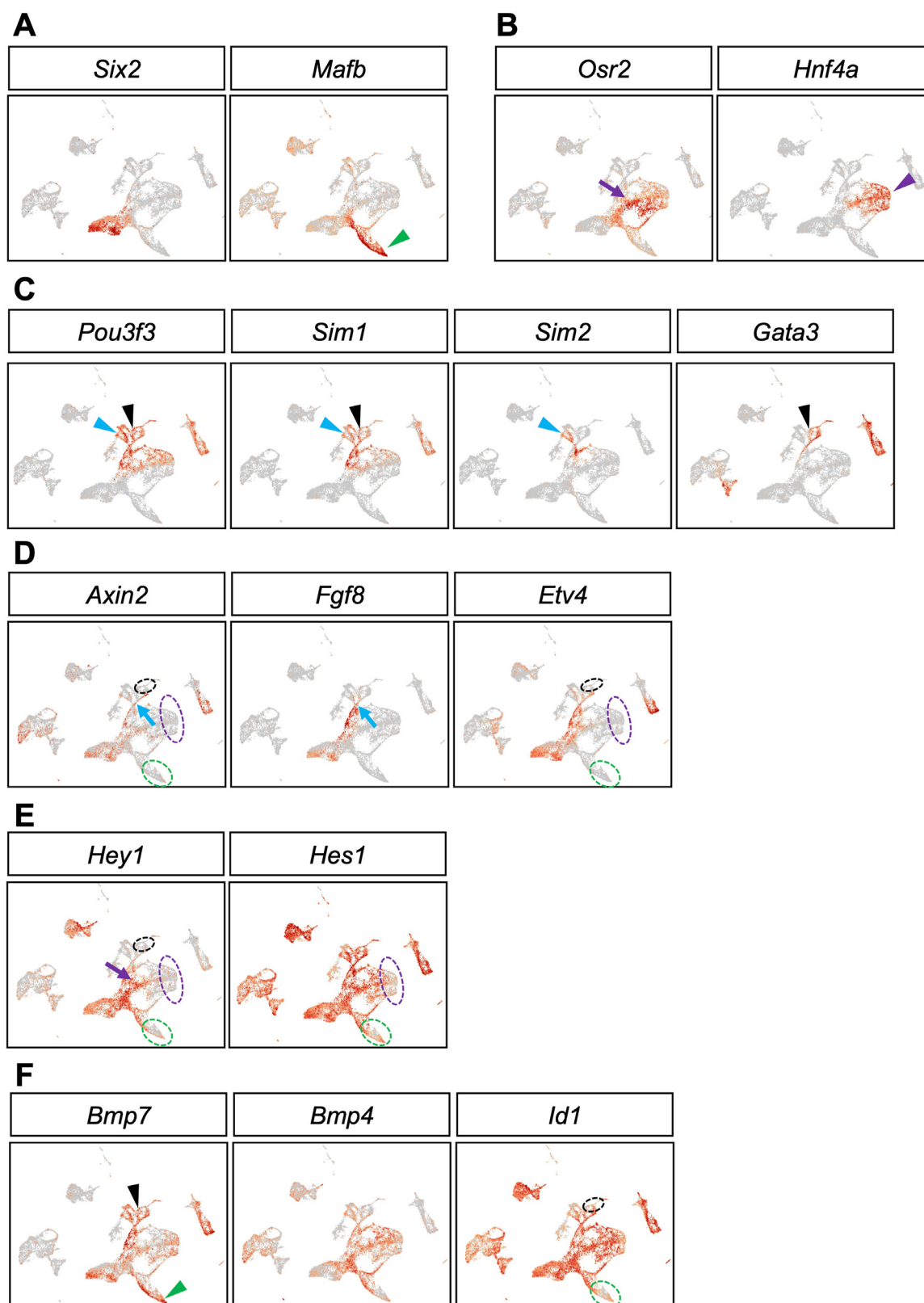
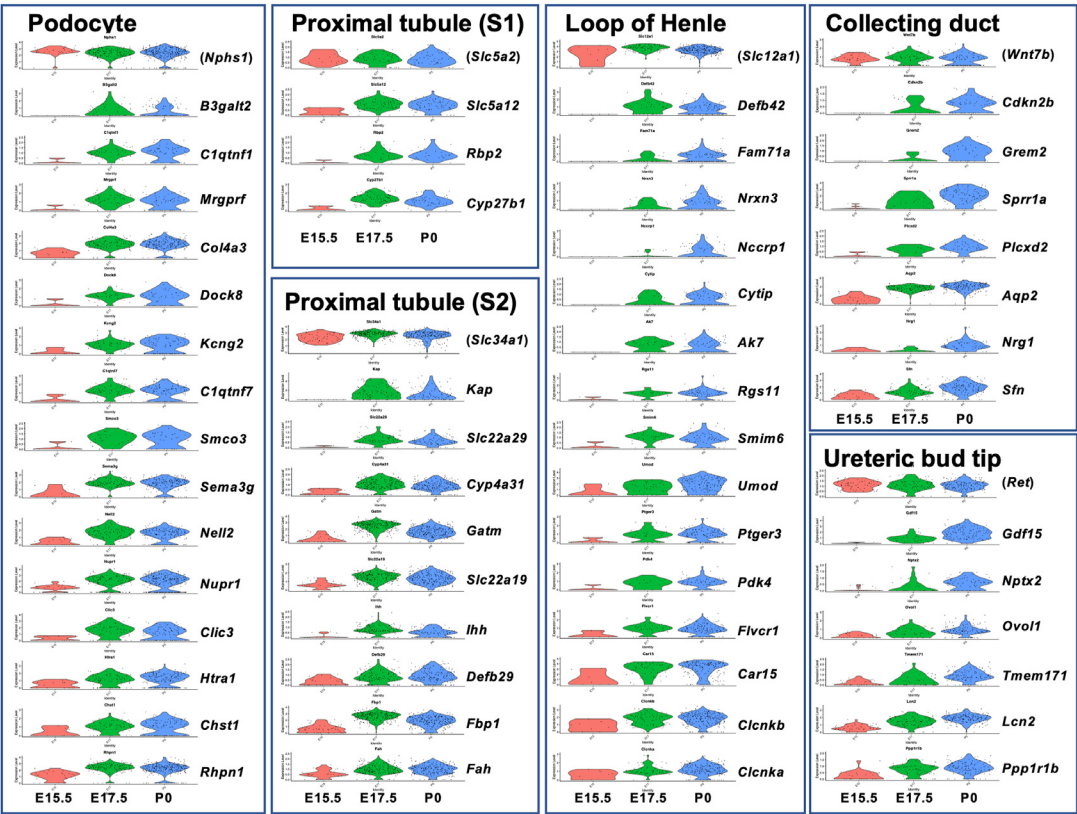


Fig. 2. Temporal changes in transcription factor expressions and developmental signaling activities during kidney maturation. (A–C) Stage-merged UMAP plots for cell type-specific marker genes. (A) Nephron progenitor cells (*Six2*) and podocytes (*Mafb*). (B) Proximal tubules. (C) Loops of Henle and distal tubules. (D–F) Stage-merged UMAP plots for signaling indicator genes (D) *Axin2* (Wnt activity indicator), *Fgf8*, and *Etv4* (FGF activity indicator). (E) Notch signaling indicator genes. (F) BMP signaling-related genes. Green arrowhead: podocyte; purple arrow and arrowhead: immature and mature proximal tubule, respectively; blue arrowhead: loop of Henle; black arrowhead: distal tubule; blue arrow: precursor cells of LOH and distal tubule. Dotted circles indicate downregulation of signaling indicator genes in mature populations.

A



B

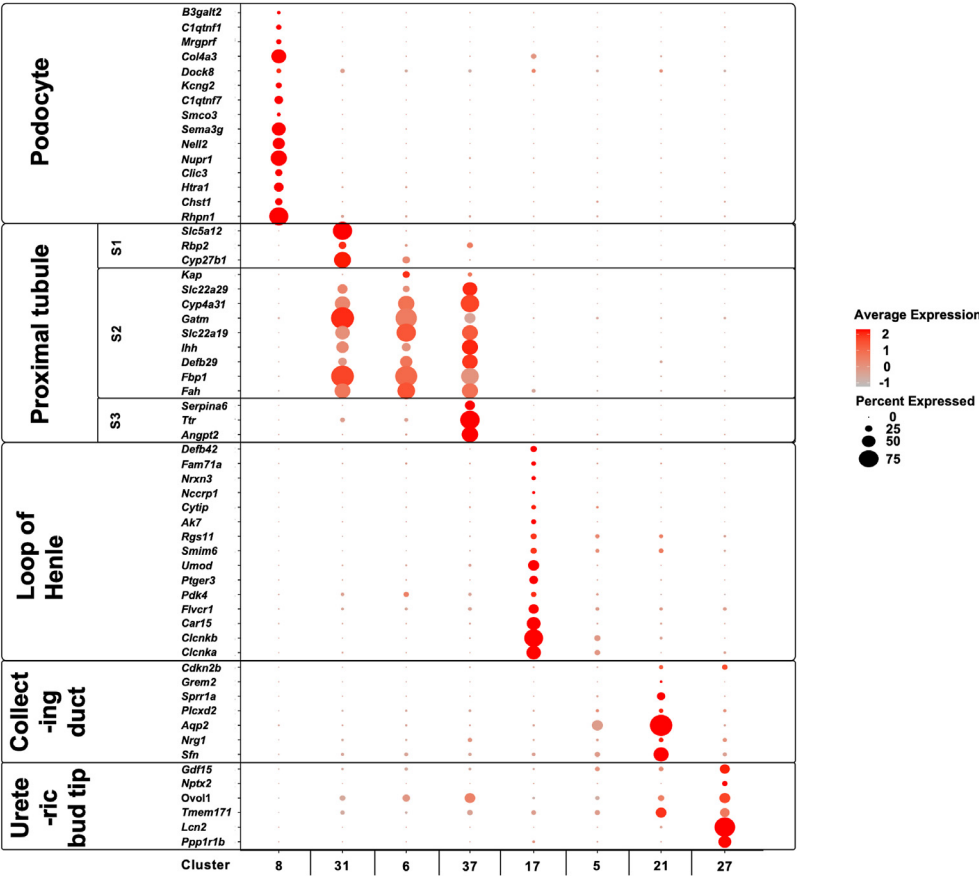


Fig. 3. Selection of stage-dependent genes during kidney maturation. Expression patterns of stage-dependent genes in the scRNA-seq data. (A) Violin plots showing stage-dependent expressions. X-axis: percentage of cells with an indicated gene expression level; Y-axis: gene expression level in each cell. (B) Dot plots showing lineage-dependent expressions. Dot color intensities represent absolute expression values and dot sizes represent percentages of cells expressing an indicated gene.

and showed comparable expression levels to those at P0, suggesting that substantial maturation may occur between E15.5 and E17.5. We detected only a few genes for distal tubules (Table S1), because most of the upregulated genes in this cell lineage were also expressed in collecting ducts. Taken together, scRNA-seq analysis of developing kidneys at multiple maturation stages enabled the identification of stage-dependent and lineage-specific genes in most nephron segments.

2.4. Histological validation of stage-dependent gene expressions of representative genes

To confirm the validity of the gene lists by histological examination, we determined the expressions of selected genes in E15.5 and P0 kidneys by conventional digoxigenin-based *in situ* hybridization or highly sensitive RNAscope technology (Wang et al., 2012). Because *in situ* hybridization, and especially RNAscope technology, involves extensive signal amplification, it is unlikely to detect subtle differences in gene expression levels. Thus, we selected genes that showed minimal expression at E15.5 and were restricted to a single lineage at P0 in the UMAP plots. Such genes would also be useful for cost-effective assessment of maturation stages using histological sections. In podocytes, all four genes examined (*Col4a3*, *Sema3g*, *Htra1*, *Clic3*) were readily detected at P0, and their expression levels at E15.5 were lower than those at P0 (Fig. 4A). In contrast, *Nphs1* showed comparable expression at the two stages (Fig. 4A). In proximal tubules, three genes (*Slc5a12*, *Cyp27b1*, *Kap*) showed weak or minimal signals at E15.5 and strong expression at P0 (Fig. 4B), while *Slc34a1* showed comparable expression at both stages (Fig. 4B). Stage-dependent expressions of three genes were validated in LOH (*Umod*, *Ptger3*, *Car15*), in contrast to the relatively constant expression of *Slc12a1* (Fig. 5A). We also performed *in situ* hybridization for three genes (*Aqp2*, *Cdkn2b*, *Lcn2*) in collecting ducts, and confirmed their stage-dependent expressions (Fig. 5B). Among these, *Aqp2* and *Cdkn2b* were expressed in collecting duct stalks, while *Lcn2* was detected in ureteric bud tips. In contrast, *Ret* and *Wnt7b* showed relatively constant expression levels (Fig. 5B). The *in situ* hybridization data were consistent with the UMAP plots, supporting the reliability of our scRNA-seq data.

2.5. Transplanted embryonic kidneys show maturation close to the neonatal stage

To determine whether transplanted kidneys followed the physiological maturation process, we performed transplantation experiments using embryonic mouse kidneys as donor tissues. Because transplantation of isolated embryonic kidneys caused hydronephrosis likely resulting from urinary tract misconnection (Fig. S5A), we used a previously reported protocol that potentially preserves the intact urinary flow (Yokote et al., 2015). For this, we transplanted E12.5 kidneys connected with the cloaca, precursor of the bladder, into the epididymis fat of host adult mice (Fig. 6A). When harvested at 12 days after transplantation, the kidneys had increased in size ($3.29 \pm 0.35 \text{ mm}^2$ vs. $0.23 \pm 0.02 \text{ mm}^2$, $n = 3$, $p < 0.05$), and urine was detected in the bladder (Fig. 6A), suggesting that the urinary flow through the kidney-bladder connection was maintained. Histological analysis showed that the renal medulla was formed with corticomedullary patterning (Fig. 6A). Staining of cell type-specific markers indicated that the overall distribution of LTL + proximal tubules, SLC12A1 + LOH, and KRT8 + ureteric buds was preserved (Fig. 6B), and that glomeruli with NPHS1 + podocytes were vascularized with PECAM1 + endothelial cells (Fig. S5B), which is rarely observed during *in vitro* culture of embryonic kidneys (Halt et al., 2016).

Next, we performed scRNA-seq analysis of transplanted embryonic kidneys and compared the data with those obtained from embryonic kidneys *in vivo*. The UMAP plots of the transplanted kidneys showed similar cluster patterns to those of neonatal kidneys *in vivo* (Fig. 6C), but the clusters representing the nephron progenitors and ureteric bud tips were missing in the transplanted kidneys (Fig. 6C, Figs. S5C and D). Although the reason for this unexpected depletion of the nephrogenic

niche remains unknown, it may explain the smaller size of transplanted kidneys compared with kidneys *in vivo*, as we discuss in a later section. Nonetheless, the other cell populations were clustered into similar patterns to those in kidneys at the neonatal stage (Fig. 6C). The expression levels of most maturation-dependent genes in podocytes and proximal tubules in the transplanted kidneys were comparable to those in P0 kidneys (Fig. 6D, Fig. S6, Table S2). However, many genes in the collecting ducts were expressed at lower levels than those in P0 kidneys, including *Cdkn2b* (Fig. 6D, Fig. S6, Table S2). In contrast, *Aqp2* and *Aqp3* expressions were relatively maintained at comparable levels to those in P0 kidneys (Fig. 6D). In addition, *Wnt9b* and *Hoxd3*, which were downregulated at P0 *in vivo*, remained high in the transplanted kidneys (Fig. S4A). Thus, the collecting ducts in the transplanted kidneys were likely to be more immature than kidneys at P0. A similar tendency, albeit to a lesser extent, was observed in LOH (Fig. 6D, Fig. S6). These results suggest that maturation does not necessarily occur synchronously across all cell lineages.

3. Discussion

Organ maturation is one of the most important aspects in developmental biology. In stem cell biology, transplantation is frequently utilized to induce maturation of pluripotent stem cell-derived organoids, including kidney organoids. However, precise determination of maturation stages is difficult because of the lack of molecular coordinates for maturation. Thus, we performed scRNA-seq analysis of mouse embryonic kidneys at different developmental stages, which enabled the identification of genes that showed stage-dependent expression in maturing embryonic kidneys. By applying this information to scRNA-seq data in transplanted embryonic kidneys, we further found that the maturation process after transplantation proceeded close to the neonatal stage, but non-synchronously across cell lineages. Unlike bulk sequencing, scRNA-seq was able to assess gene expressions in the most mature fractions of each cell lineage, thus enabling precise comparisons with the corresponding subpopulations in developing kidneys as well as in transplanted kidneys. The selected gene lists for stage-dependent expressions were proven to function as molecular coordinates for assessment of the maturation stages of individual lineages. Addition of scRNA-seq data in postnatal kidneys at different stages and adult kidneys would create further useful resources for maturation assessment.

To determine whether similar results can be achieved using the pre-existing datasets, we reanalyzed the published scRNA-seq data in E14.5 and P1 kidneys (Adam et al., 2017a; Magella et al., 2017). However, UMAP plots showed that the clusters representing the mature populations of most cell types at P1 were absent in the E14.5 data (Figs. S7A and B), thereby hindering us from comparing gene expression in the corresponding clusters between the two stages. The only exception was ureteric bud tips. *Ret* + clusters were detected at both stages, and *Lcn2* was upregulated at P1 (Fig. S7C), consistent with our results. Thus, the pre-existing data were of limited use, emphasizing the importance of the scRNA-seq data and gene lists in the present study.

We showed that podocytes and proximal tubules in the transplanted kidneys matured close to the neonatal stage, while collecting ducts remained relatively immature. The underlying reasons for the maturation impairment of the collecting ducts remain to be elucidated. A reduction in physical force evoked by urinary flow may be one possible reason, because the collecting ducts are located furthest downstream in the urinary tract. We transplanted embryonic kidneys with the cloaca, with the aim of better urinary flow preservation compared with conventional transplantation of isolated kidneys (Fig. S5). However, it remains possible that the urinary flow was insufficient to promote maturation of the lower part of the nephron segments. Alternatively, the collecting ducts may already have suffered mechanical damage caused by backflow from the bladder, although apparent hydronephrosis or hydronephrosis was not observed at the time of the analysis. Subsequent connection of the donor-derived bladder with the host ureter was

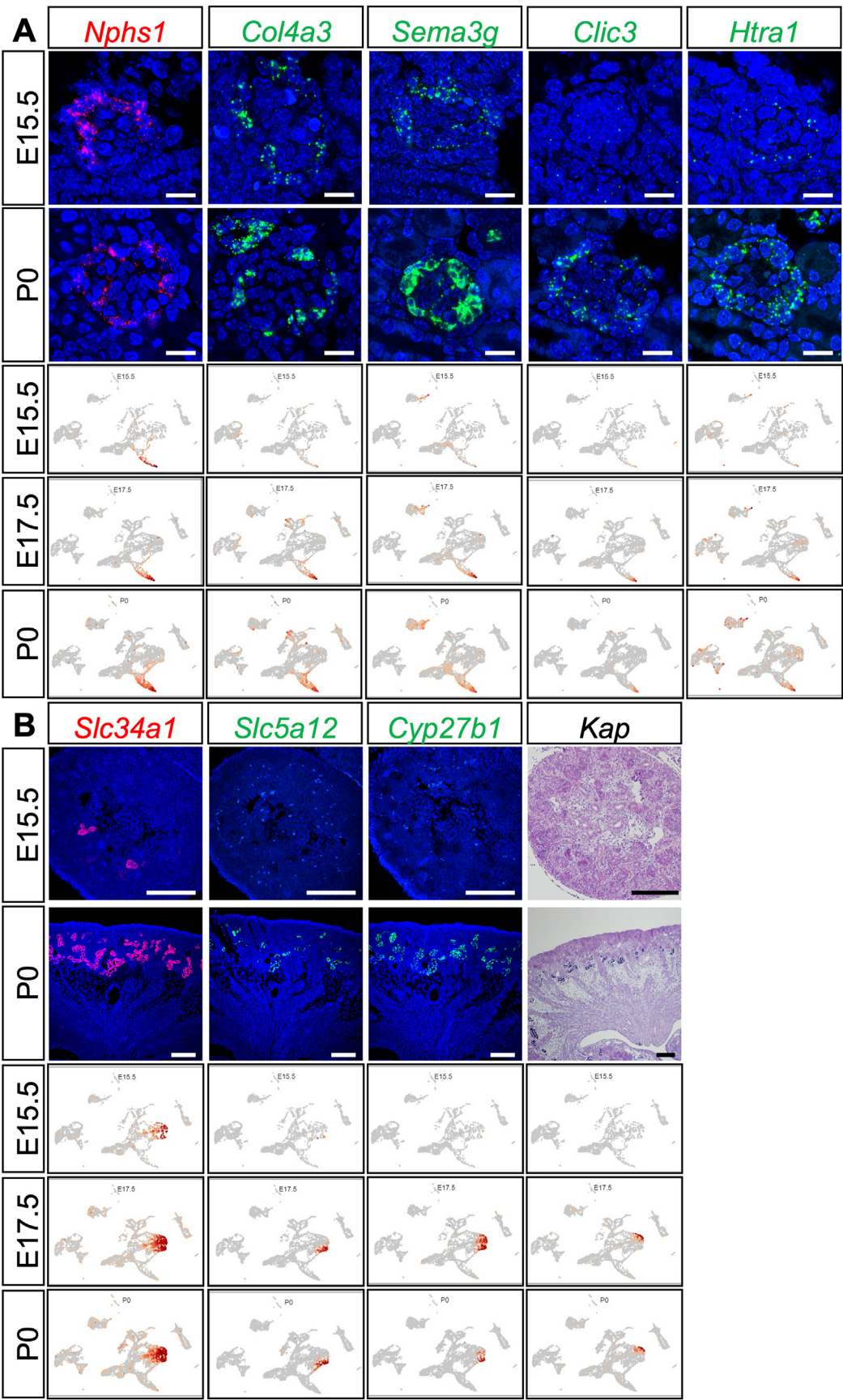


Fig. 4. Validation of stage-dependent gene expressions during podocyte and proximal tubule maturation. *In situ* hybridization (upper two rows) validated the results of the UMAP plots (lower three rows). (A) Podocyte genes. Confocal images of RNAscope *in situ* hybridization with adjacent sections. Scale bar: 20 μ m. (B) Proximal tubule genes. Confocal images of RNAscope *in situ* hybridization with adjacent sections except for *Kap*, in which bright-field images of digoxigenin-mediated *in situ* hybridization are shown. Scale bar: 200 μ m. *Nphs1* and *Slc34a1* are stage-independent segment-specific markers for podocytes and proximal tubules, respectively.

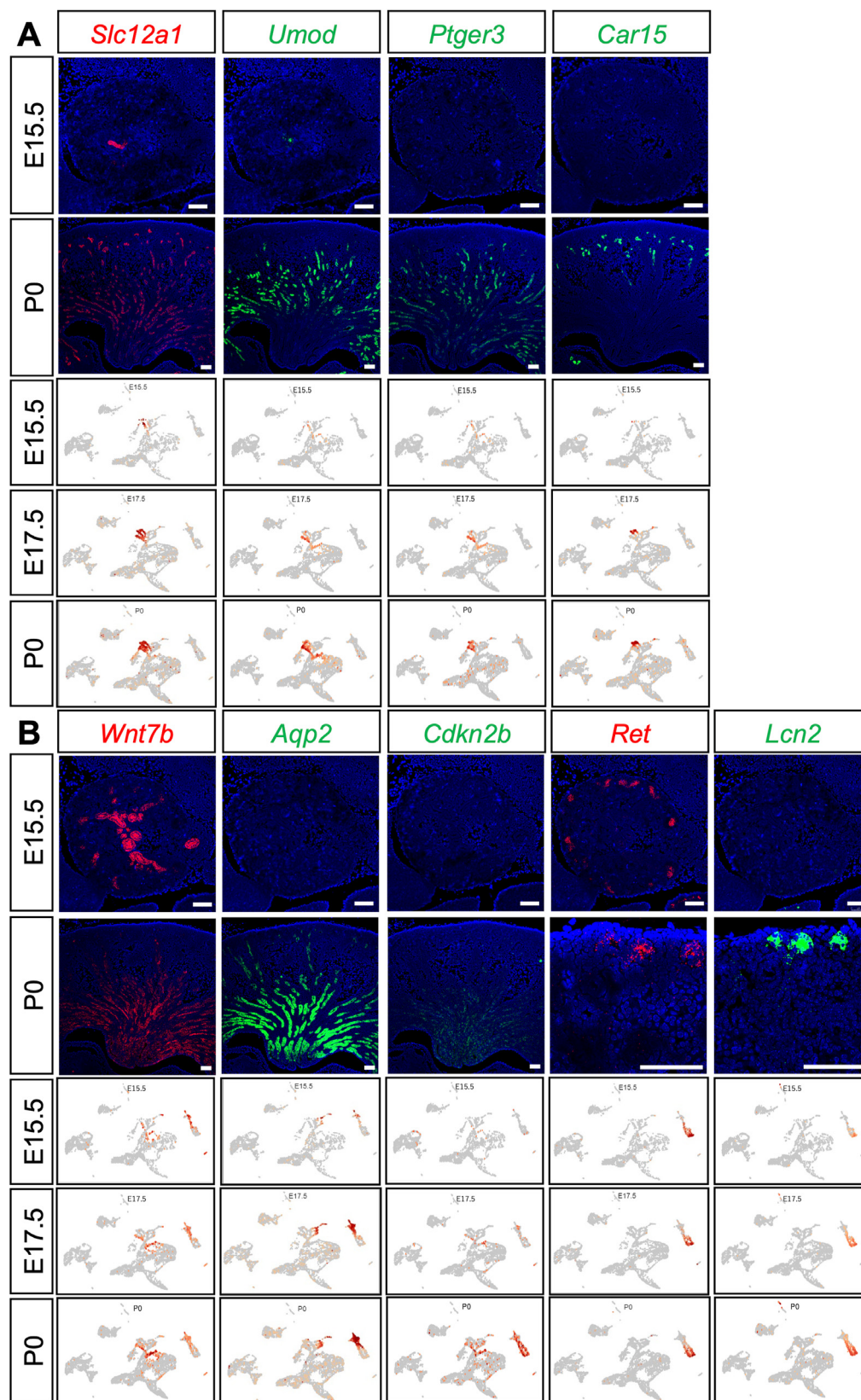


Fig. 5. Validation of stage-dependent gene expressions during maturation of loops of Henle (LOH) and collecting ducts. Confocal images of RNAscope *in situ* hybridization with adjacent sections (upper two rows) validated the results of the UMAP plots (lower three rows). (A) Genes for LOH. (B) Genes for collecting duct stalks (left three columns) and ureteric bud tips (right two columns). *Slc12a1*, *Wnt7b*, and *Ret* are stage-independent lineage-specific markers for LOH, collecting duct stalks, and ureteric bud tips, respectively. Scale bar: 100 μ m.

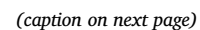


Fig. 6. Maturation of transplanted kidneys close to the neonatal stage. (A) Whole-mount view of an E12.5 kidney with the cloaca before transplantation (day 0). Whole-mount view and histological analysis with hematoxylin and eosin staining of the transplanted kidney with the bladder harvested at day 12 after transplantation. Red arrow: presence of urine in the bladder. Scale bar: 500 μ m. (B) Immunostaining of the kidney at day 12 after transplantation with markers for proximal tubules (LTL: green), loops of Henle (SLC12A1: red), and collecting ducts (KRT8: grey). Scale bar: 200 μ m. (C) UMAP plots of embryonic kidneys *in vivo* (E15.5 and P0) and transplanted embryonic kidneys (day 12 after transplantation). Arrow: nephron progenitor (NP); arrowhead: ureteric bud tip (UB). POD: podocyte; PEC: glomerular parietal epithelial cell; DN: differentiating nephron; PT: proximal tubule; LOH: loop of Henle; DT: distal tubule; CD: collecting duct; CD-IC: intercalated cell of collecting duct; IC: interstitial cell; EC: endothelial cell; UT: ureter; BC: blood cell. (D) Violin plots of stage-dependent genes in transplanted kidneys compared with embryonic kidneys *in vivo* (E15.5 and P0).

reported to inhibit hydronephrosis and assisted further development (Yokote et al., 2015), thus it would be informative to analyze the expressions of our maturation marker genes in such transplants. While further studies are needed, our gene lists were proven useful for assessment of the maturation status of individual lineages in developing kidneys as well as in transplanted kidneys.

Our RNA-seq data will also serve as useful coordinates to assess the maturation status of kidney organoids derived from pluripotent stem cells. The current kidney organoids represent those at embryonic stages (Taguchi and Nishinakamura, 2017; Takasato et al., 2015; Wu et al., 2018), and further maturation is required for disease modeling and eventually for generation of transplantable kidneys. At present, few methods are available to measure the maturation stages of organoids, except for morphological analyses. Thus, our results will serve as a basis toward molecular detection of organoid maturation. While the conventional kidney organoids mainly consist of nephrons (glomeruli and renal tubules), we recently reported the generation of higher-order kidney structures, comprising branching ureteric buds with nephrons distributed around the ureteric bud tips (Taguchi and Nishinakamura, 2017). We achieved this by combining mouse ESC-derived nephron progenitors and ureteric buds with embryonic stromal progenitors, and it should be theoretically possible in the near future to generate organotypic kidney structures solely from mouse ESCs and eventually from human iPSCs. Thus, the next step would be transplantation of organoids for further maturation. Our scRNA-seq data will serve as useful reference tools to assess the maturation stages of the transplanted organoids.

The depletion of the nephrogenic niche in the transplanted kidneys was unexpected. Although not the main scope of the present study focusing on maturation, this depletion may explain the smaller size of transplanted kidneys compared with kidneys *in vivo*. Nephron progenitors in mice continue to give rise to nascent nephrons until several days after birth (Hartman et al., 2007; Rumballe et al., 2011; Volovelsky et al., 2018) and premature depletion of nephron progenitors leads to smaller-size kidneys (Kanda et al., 2014; Self et al., 2006). It remains to be determined which maintenance factors are lacking in transplanted kidneys and whether loss of nephron progenitors or ureteric bud tips is the primary cause of this phenomenon. Solving these enigmas will eventually lead to the growth of transplanted kidney organoids to a comparable size to kidneys *in vivo*.

Taken together, we have demonstrated that our scRNA-seq data and gene lists can serve as molecular bases to assess the maturation stages of embryonic and transplanted kidneys, and would be applicable to kidney organoids derived from iPSCs. Although we focused on nephron development and maturation in the present study, detailed analyses of other lineages, such as stromal and endothelial cells, using our scRNA-seq data will provide more insights into kidney maturation.

4. Materials and methods

4.1. scRNA-seq analyses

Kidneys were dissociated by a protocol modified from a previously described method (Tanigawa et al., 2016) and used for scRNA-seq analyses. C57BL/6N mice (CLEA Japan Inc.) were employed for E15.5 and E17.5 analyses, and Foxd1GFP^{CreER}; tdTomato and Tbx18MerCreMer; tdTomato mice on a mixed genetic background of C57BL/6N and ICR were used for P0 analyses (Grisanti et al., 2013; Kobayashi et al., 2014).

Six kidneys at E15.5 were digested for 10 min in 0.25% trypsin/EDTA. E17.5 and P0 female kidneys were minced roughly with forceps, digested with dissociation buffer comprising 2 mg/ml collagenase (Sigma; Cat# 9407), 2.4 U/ml dispase (Gibco; Cat# 17105-041), 2 mM CaCl₂ (Wako; Cat# 031-00435), 50 μ g/ml DNase I (Sigma; Cat# 11284932001), and 10% fetal calf serum (FCS) (Sigma; Cat# 172012) in Dulbecco's modified Eagle's medium (DMEM) (Sigma; Cat# D5796) for 15 min at 37 °C, washed with phosphate-buffered saline (PBS), and treated with 0.25% trypsin/EDTA for 10 min. Trypsin was inactivated by addition of DMEM/10% FCS containing 50 μ g/ml DNase I, and the cells were washed with HEPES-buffered saline solution (Thermo; Cat# 14185-052) containing 2% FCS, 50 μ g/ml DNase I, 1 mM CaCl₂, and 0.035% NaHCO₃ (Wako; Cat# 191-01305). Cells were resuspended in 0.04% BSA/PBS, filtered through a 40- μ m-pore strainer (Falcon; Cat# 352340), and evaluated for their cell number and viability (>90%) using a Countess automated cell counter (Thermo; Cat# C10227). A total of 5000 dissociated cells each from E15.5 and E17.5 and two samples (5000 cells per sample) from P0 were applied to Chromium Controller (10x Genomics). A Chromium Single Cell 3' Library & Gel Beads Kit v2 (10x Genomics) was used to generate oligo-dT-primed cDNA libraries, which were then sequenced by an Illumina HiSeq 3000 (14,000 reads for E15.5; 7000 reads for E17.5; 14,000 reads for P0). The Q30 base RNA reads (Q-scores indicating sequencing quality) of the samples were 86.2% for E15.5, 63.8% for E17.5, and 93.6% for P0.

The raw sequence data were processed using the *cell ranger count* command of Cell Ranger (version 3.0.2; 10x Genomics) to generate count tables of unique molecular identifiers (UMIs) for each gene per cell. First, we integrated the two P0 samples using the *cell ranger aggr* command of Cell Ranger to generate a single combined P0 sample. At this point, we obtained 4,158, 5,551, and 10,810 cells for the E15.5, E17.5, and P0 samples with medium reads of 4,493, 2,360, and 2467 genes per cell, respectively. These three individually generated datasets were integrated using the *cell ranger aggr* command. All subsequent analyses were performed in the R statistical programming language (R Core Team, 2018). The Seurat package (version 3.1.1) was used for analyses including quality control, data normalization, data scaling, and visualization (Butler et al., 2018) (Stuart et al., 2019a). For quality control, cells that expressed <200 genes, >8000 genes (possibly representing doublets), or >20% of mitochondrial genes were filtered out. The final dataset contained 20,672 genes and 3,441, 4,592, and 8161 cells in the E15.5, E17.5, and P0 samples, respectively (total: 16,194 cells). A principal component analysis was used for dimension reduction with a dimension value of 74 determined by the JackStrawPlot function (Chung and Storey, 2015). The top 2000 highly variable genes were selected by the FindVariableFeatures function and used together with dimensional information for clustering. Cluster segmentation was performed using a resolution value of 2.4. The FindClusters command generated a total of 45 clusters that were easily distinguished with cluster-specific marker genes obtained with the FindMarkers function of the Seurat package. Cluster 26 probably consisted of dying cells that escaped from the filtering parameters, because it showed no specific marker genes, low mitochondrial genes, and relatively low number of features. Uniform Manifold Approximation and Projection for Dimension Reduction (UMAP) plots were generated using the uwot package (Becht et al., 2019). The UMAP coordinates, Seurat cluster coordinates, and cluster-specific markers obtained were exported as csv files for confirmation analysis using Loupe Cell Browser software (10x Genomics). The scRNA-seq data were deposited in the

National Center for Biotechnology Information Gene Expression Omnibus (GSE149134).

4.2. Selection of developmental stage-dependent gene candidates

To select developmental stage-dependent gene candidates in each cluster, we used the FindMarkers function to pick up genes that were upregulated at P0 compared with E15.5 (e.g. comparison between cluster 8 at P0 and cluster 8 at E15.5 for podocytes). Subsequently, we utilized the AverageExpression function to add the average gene expression data for each cluster at each stage for stage-dependent comparisons (log-fold change >1 and p-value <0.05). To determine segment-specific genes, we compared the target cluster with all other clusters at P0 and selected the genes with low p-values ($p < 0.05$) and low expression rates in other clusters (pct2 <0.11). After selecting the overlapping genes, we verified them in UMAP plots to finalize the lineage-specific stage-dependent genes.

4.3. Immunohistochemical analysis

Paraffin sections were subjected to antigen retrieval in a citrate buffer, washed three times with PBS, and blocked by incubation with 1% BSA in PBS for 1 h at room temperature. The sections were then incubated overnight with primary antibodies at 4 °C, followed by incubation with secondary antibodies conjugated with Alexa Fluor dyes for 90 min at room temperature. Nuclei were stained with 4,6-diamidino-2-phenylindole (Roche; Cat# 10236276001). The following primary antibodies were used: biotinylated LTL (Vector Laboratories; B-1325), rabbit anti-SLC12A1 (StressMarq Bioscience; SPC-401D), rat anti-KRT8 (Developmental Studies Hybridoma Bank, University of Iowa; Troma-I), guinea pig anti-NPHS1 (Progen; GP-N2); and rabbit anti-CD31 (Abcam; ab28364). Fluorescence images were captured by an LSM780 confocal microscope (Carl Zeiss) or FV3000 confocal microscope (Olympus).

4.4. In situ hybridization

RNAscope analysis of 10% formalin-fixed paraffin sections was performed using an RNAscope Multiplex Fluorescent Reagent Kit v2 (ADC; Cat# 323100). Signal amplification was performed with TSA plus fluorophores (Thermo Fisher Scientific). Details of the RNAscope probes are provided in Table S3. Digoxigenin-based *in situ* hybridization of *Kap* was performed as described (Kaku et al., 2013) using an automated Discovery System (Roche), according to the manufacturer's protocols. The *Kap* probe was cloned by PCR using specific primers (Table S3), and labeled with digoxigenin using an RNA polymerase. Two to three samples at each embryonic stage were examined for each probe, and showed consistent results.

4.5. Transplantation of mouse embryonic kidneys

C57BL/6N pregnant female mice (E12.5) and adult male mice (8–12 weeks) were purchased from CLEA Japan Inc. and housed in a specific pathogen-free animal facility. Host adult mice were anesthetized by peritoneal administration of normal saline containing 0.75 mg/kg medetomidine, 4.0 mg/kg midazolam, and 5.0 mg/kg butorphanol. Mouse embryonic kidneys with the cloaca at E12.5 were transplanted into the epididymis fat of host mice (Yokote et al., 2015). After surgery, atipamezole was administered as an anesthetic antagonist. The transplanted embryonic kidneys were harvested at 12 days after transplantation. For scRNA-seq analysis, the kidneys were dissociated similarly to the P0 kidneys. All animal experiments were carried out in accordance with our institutional guidelines and were approved by the Ethics Committee of Kumamoto University (#A2019-113).

4.6. Re-analysis of the publicly available scRNA-seq data

The scRNA-seq data for E14.5 mouse embryonic kidney and P1 kidney (Adam et al., 2017b; Magella et al., 2017) were downloaded from the Gene Expression Omnibus (Accession Numbers, GSE94333 and GSE104396, respectively). All subsequent analyses of these data were performed in the R statistical programming language (R Core Team, 2018), and the Seurat package (version 3.2.2) was used for analyses including quality control, data normalization, data scaling, and visualization as described in Section 4.1.

Acknowledgments

We thank Sayoko Fujimura, Shingo Usuki, and Itoshi Nikaido for technical assistance and advice. We also thank Alison Sherwin, PhD, from Edanz Group (<https://en-author-services.edanzgroup.com/ac>) for editing a draft of this manuscript. The study was supported, in part, by a KAKENHI grant (JP17H06177 to R.N.) from the Japan Society for the Promotion of Science.

Appendix A. Supplementary data

Supplementary data to this article can be found online at <https://doi.org/10.1016/j.ydbio.2020.11.002>.

References

- Adam, M., Potter, A.S., Potter, S.S., 2017a. Psychrophilic proteases dramatically reduce single-cell RNA-seq artifacts: a molecular atlas of kidney development. *Development* 144, 3625–3632. <https://doi.org/10.1242/dev.151142>.
- Adam, M., Potter, A.S., Potter, S.S., 2017b. Psychrophilic proteases dramatically reduce single-cell RNA-seq artifacts: a molecular atlas of kidney development. *Development* 144, 3625–3632. <https://doi.org/10.1242/dev.151142>.
- Bantounas, I., Ranjzad, P., Tengku, F., Silajdzic, E., Forster, D., Asselin, M.-C., Lewis, P., Lennon, R., Plagge, A., Wang, Q., Woolf, A.S., Kimber, S.J., 2018. Generation of functioning nephrons by implanting human pluripotent stem cell-derived kidney progenitors. *Stem Cell Reports* 10, 766–779. <https://doi.org/10.1016/j.stemcr.2018.01.008>.
- Becht, E., McInnes, L., Healy, J., Dutertre, C.-A., Kwok, I.W.H., Ng, L.G., Ginhoux, F., Newell, E.W., 2019. Dimensionality reduction for visualizing single-cell data using UMAP. *Nat. Biotechnol.* 37, 38–44. <https://doi.org/10.1038/nbt.4314>.
- Boyle, S., Misfeldt, A., Chandler, K.J., Deal, K.K., Southard-Smith, E.M., Mortlock, D.P., Baldwin, H.S., de Caestecker, M., 2008. Fate mapping using Cited1-CreERT2 mice demonstrates that the cap mesenchyme contains self-renewing progenitor cells and gives rise exclusively to nephronic epithelia. *Dev. Biol.* 313, 234–245. <https://doi.org/10.1016/j.ydbio.2007.10.014>.
- Butler, A., Hoffman, P., Smibert, P., Papalexi, E., Satija, R., 2018. Integrating single-cell transcriptomic data across different conditions, technologies, and species. *Nat. Biotechnol.* 36, 411–420. <https://doi.org/10.1038/nbt.4096>.
- Chen, S., Brunskill, E.W., Potter, S.S., Dexheimer, P.J., Salomonis, N., Aronow, B.J., Hong, C.I., Zhang, T., Kopan, R., 2015. Intrinsic age-dependent changes and cell-cell contacts regulate nephron progenitor lifespan. *Dev. Cell* 35, 49–62. <https://doi.org/10.1016/j.devcel.2015.09.009>.
- Chung, N.C., Storey, J.D., 2015. Statistical significance of variables driving systematic variation in high-dimensional data. *Bioinformatics* 31, 545–554. <https://doi.org/10.1093/bioinformatics/btu674>.
- Combes, A.N., Phipson, B., Lawlor, K.T., Dorison, A., Patrick, R., Zappia, L., Harvey, R.P., Oshlack, A., Little, M.H., 2019a. Single cell analysis of the developing mouse kidney provides deeper insight into marker gene expression and ligand-receptor crosstalk. *Development* 146, dev178673. <https://doi.org/10.1242/dev.178673>.
- Combes, A.N., Zappia, L., Er, P.X., Oshlack, A., Little, M.H., 2019b. Single-cell analysis reveals congruence between kidney organoids and human fetal kidney. *Genome Med.* 11, 3. <https://doi.org/10.1186/s13073-019-0615-0>.
- Costantini, F., Kopan, R., 2010. Patterning a complex organ: branching morphogenesis and nephron segmentation in kidney development. *Dev. Cell* 18, 698–712. <https://doi.org/10.1016/j.devcel.2010.04.008>.
- Deacon, P., Concodora, C.W., Chung, E., Park, J.-S., 2019. β -catenin regulates the formation of multiple nephron segments in the mouse kidney. *Sci. Rep.* 9, 15915. <https://doi.org/10.1038/s41598-019-52255-w>.
- Grisanti, L., Clavel, C., Cai, X., Rezza, A., Tsai, S.-Y., Sennett, R., Mumau, M., Cai, C.-L., Rendl, M., 2013. Tbx18 targets dermal condensates for labeling, isolation, and gene ablation during embryonic hair follicle formation. *J. Invest. Dermatol.* 133, 344–353. <https://doi.org/10.1038/jid.2012.329>.
- Halt, K.J., Pärssinen, H.E., Junttila, S.M., Saarela, U., Sims-Lucas, S., Koivunen, P., Myllyharju, J., Quaggin, S., Skovorodkin, I.N., Vainio, S.J., 2016. CD146 + cells are essential for kidney vasculature development. *Kidney Int.* 90, 311–324. <https://doi.org/10.1016/j.kint.2016.02.021>.

- Hartman, H.A., Lai, H.L., Patterson, L.T., 2007. Cessation of renal morphogenesis in mice. *Dev. Biol.* 310, 379–387. <https://doi.org/10.1016/j.ydbio.2007.08.021>.
- Jho, E., Zhang, T., Dorn, C., Joo, C.-K., Freund, J.-N., Costantini, F., 2002. Wnt/ β -catenin/Tcf signaling induces the transcription of Axin2, a negative regulator of the signaling pathway. *Mol. Cell Biol.* 22, 1172–1183. <https://doi.org/10.1128/mcb.22.4.1172-1183.2002>.
- Kaku, Y., Ohmori, T., Kudo, K., Fujimura, S., Suzuki, K., Evans, S.M., Kawakami, Y., Nishinakamura, R., 2013. Islet1 deletion causes kidney agenesis and hydronephrosis resembling CAKUT. *J. Am. Soc. Nephrol.* 24, 1242–1249. <https://doi.org/10.1681/ASN.2012050528>.
- Kanda, S., Tanigawa, S., Ohmori, T., Taguchi, A., Kudo, K., Suzuki, Y., Sato, Y., Hino, S., Sander, M., Perantoni, A.O., Sugano, S., Nakao, M., Nishinakamura, R., 2014. Sall1 maintains nephron progenitors and nascent nephrons by acting as both an activator and a repressor. *J. Am. Soc. Nephrol.* 25, 2584–2595. <https://doi.org/10.1681/ASN.2013080896>.
- Kobayashi, A., Mugford, J.W., Krautzbeger, A.M., Naiman, N., Liao, J., McMahon, A.P., 2014. Identification of a multipotent self-renewing stromal progenitor population during mammalian kidney organogenesis. *Stem Cell Reports* 3, 650–662. <https://doi.org/10.1016/j.stemcr.2014.08.008>.
- Kobayashi, A., Valerius, M.T., Mugford, J.W., Carroll, T.J., Self, M., Oliver, G., McMahon, A.P., 2008. Six2 defines and regulates a multipotent self-renewing nephron progenitor population throughout mammalian kidney development. *Cell Stem Cell* 3, 169–181. <https://doi.org/10.1016/j.stem.2008.05.020>.
- Korchynski, O., Ten Dijke, P., 2002. Identification and functional characterization of distinct critically important bone morphogenetic protein-specific response elements in the Id1 promoter. *J. Biol. Chem.* 277, 4883–4891. <https://doi.org/10.1074/jbc.M111023200>.
- Lee, J.W., Chou, C.-L., Knepper, M.A., 2015. Deep sequencing in microdissected renal tubules identifies nephron segment-specific transcriptomes. *J. Am. Soc. Nephrol.* 26, 2669–2677. <https://doi.org/10.1681/ASN.2014111067>.
- Lindström, N.O., Guo, J., Kim, A.D., Tran, T., Guo, Q., De Sena Brandine, G., Ransick, A., Parvez, R.K., Thornton, M.E., Baskin, L., Grubbs, B., McMahon, J.A., Smith, A.D., McMahon, A.P., 2018. Conserved and divergent features of mesenchymal progenitor cell types within the cortical nephrogenic niche of the human and mouse kidney. *J. Am. Soc. Nephrol.* 29, 806–824. <https://doi.org/10.1681/ASN.2017080890>.
- López-Rovira, T., Chaux, E., Massagué, J., Rosa, J.L., Ventura, F., 2002. Direct binding of Smad1 and Smad4 to two distinct motifs mediates bone morphogenetic protein-specific transcriptional activation of Id1 gene. *J. Biol. Chem.* 277, 3176–3185. <https://doi.org/10.1074/jbc.M106826200>.
- Magella, B., Adam, M., Potter, A.S., Venkatasubramanian, M., Chetal, K., Hay, S.B., Salomonis, N., Potter, S.S., 2017. Cross-platform single cell analysis of kidney development shows stromal cells express Gdnf. *Dev. Biol.* 434, 36–47. <https://doi.org/10.1016/j.ydbio.2017.11.006>.
- Mao, J., McGlinn, E., Huang, P., Tabin, C.J., McMahon, A.P., 2009. Fgf-dependent Etv4/5 activity is required for posterior restriction of Sonic hedgehog and promoting outgrowth of the vertebrate limb. *Dev. Cell* 16, 600–606. <https://doi.org/10.1016/j.devcel.2009.02.005>.
- Marable, S.S., Chung, E., Adam, M., Potter, S.S., Park, J.-S., 2018. Hnf4a deletion in the mouse kidney phenocopies Fanconi renal tubular syndrome. *JCI Insight* 3, e97497. <https://doi.org/10.1172/jci.insight.97497>.
- Marable, S.S., Chung, E., Park, J.-S., 2020. Hnf4a is required for the development of Cdh6-expressing progenitors into proximal tubules in the mouse kidney. *J. Am. Soc. Nephrol.* 31, 2543–2558. <https://doi.org/10.1681/ASN.2020020184>.
- Marneros, A.G., 2020. AP-2 β /KCTD1 control distal nephron differentiation and protect against renal fibrosis. *Dev. Cell* 54, 348–366. <https://doi.org/10.1016/j.devcel.2020.05.026> e5.
- Marose, T.D., Merkel, C.E., McMahon, A.P., Carroll, T.J., 2008. β -catenin is necessary to keep cells of ureteric bud/Wolffian duct epithelium in a precursor state. *Dev. Biol.* 314, 112–126. <https://doi.org/10.1016/j.ydbio.2007.11.016>.
- Martovetsky, G., Tee, J.B., Nigam, S.K., 2013. Hepatocyte nuclear factors 4 and 1 regulate kidney developmental expression of drug-metabolizing enzymes and drug transporters. *Mol. Pharmacol.* 84, 808–823. <https://doi.org/10.1124/mol.113.088229>.
- McMahon, A.P., Aronow, B.J., Davidson, D.R., Davies, J.A., Gaido, K.W., Grimmond, S., Lessard, J.L., Little, M.H., Potter, S.S., Wilder, E.L., others, 2008. GUDMAP: the genitourinary developmental molecular anatomy project. *J. Am. Soc. Nephrol.* 19, 667–671. <https://doi.org/10.1681/ASN.2007101078>.
- Miyazaki, Y., Oshima, K., Fogo, A., Hogan, B.L., Ichikawa, I., 2000. Bone morphogenetic protein 4 regulates the budding site and elongation of the mouse ureter. *J. Clin. Invest.* 105, 863–873. <https://doi.org/10.1172/JCI8256>.
- Morizane, R., Lam, A.Q., Freedman, B.S., Kishi, S., Valerius, M.T., Bonventre, J.V., 2015. Nephron organoids derived from human pluripotent stem cells model kidney development and injury. *Nat. Biotechnol.* 33, 1193–1200. <https://doi.org/10.1038/nbt.3392>.
- Nakai, S., Sugitani, Y., Sato, H., Ito, S., Miura, Y., Ogawa, M., Nishi, M., Jishage, K.I., Minowa, O., Noda, T., 2003. Crucial roles for Brn1 in distal tubule formation and function in mouse kidney. *Development* 130, 4751–4759. <https://doi.org/10.1242/dev.00666>.
- Oxburgh, L., Dudley, A.T., Godin, R.E., Koonce, C.H., Islam, A., Anderson, D.C., Bikoff, E.K., Robertson, E.J., 2005. BMP4 substitutes for loss of BMP7 during kidney development. *Dev. Biol.* 286, 637–646. <https://doi.org/10.1016/j.ydbio.2005.08.024>.
- Patrakka, J., Xiao, Z., Nukui, M., Takemoto, M., He, L., Oddsson, A., Perisic, L., Kaukinen, A., Szegedy, C.A.K., Uhlén, M., Jalanko, H., Betsholtz, C., Tryggvason, K., 2007. Expression and subcellular distribution of novel glomerulus-associated proteins dendrin, Ehd3, Sh2d4a, Plekhh2, and 2310066E14Rik. *J. Am. Soc. Nephrol.* 18, 689–697. <https://doi.org/10.1681/ASN.2006060675>.
- R Core Team, 2018. R: A Language and Environment for Statistical Computing. R Foundation for statistical computing, Vienna, Austria.
- Ransick, A., Lindström, N.O., Liu, J., Zhu, Q., Guo, J.-J., Alvarado, G.F., Kim, A.D., Black, H.G., Kim, J., McMahon, A.P., 2019. Single-cell profiling reveals sex, lineage, and regional diversity in the mouse kidney. *Dev. Cell* 51, 399–413.e7. <https://doi.org/10.1016/j.devcel.2019.10.005>.
- Rasouly, H.M., Lu, W., 2013. Lower urinary tract development and disease. *Wiley Interdiscip. Rev. Syst. Biol. Med.* 5, 307–342. <https://doi.org/10.1002/wsbm.1212>.
- Rumballe, B. a, Georgas, K.M., Combes, A.N., Ju, A.L., Gilbert, T., Little, M.H., 2011. Nephron formation adopts a novel spatial topology at cessation of nephrogenesis. *Dev. Biol.* 360, 110–122. <https://doi.org/10.1016/j.ydbio.2011.09.011>.
- Self, M., Lagutin, O.V., Bowling, B., Hendrix, J., Cai, Y., Dressler, G.R., Oliver, G., 2006. Six2 is required for suppression of nephrogenesis and progenitor renewal in the developing kidney. *EMBO J.* 25, 5214–5228. <https://doi.org/10.1038/sj.emboj.7601381>.
- Sharmin, S., Taguchi, A., Kaku, Y., Yoshimura, Y., Ohmori, T., Sakuma, T., Mukoyama, M., Yamamoto, T., Kurihara, H., Nishinakamura, R., 2016. Human induced pluripotent stem cell-derived podocytes mature into vascularized glomeruli upon experimental transplantation. *J. Am. Soc. Nephrol.* 27, 1778–1791. <https://doi.org/10.1681/ASN.2015010096>.
- Stuart, T., Butler, A., Hoffman, P., Hafemeister, C., Papalexi, E., Mauck, W.M., Hao, Y., Stoeckius, M., Smibert, P., Satija, R., 2019a. Comprehensive integration of single-cell data. *Cell* 177, 1888–1902.e21. <https://doi.org/10.1016/j.cell.2019.05.031>.
- Stuart, T., Butler, A., Hoffman, P., Hafemeister, C., Papalexi, E., Mauck, W.M., Hao, Y., Stoeckius, M., Smibert, P., Satija, R., 2019b. Comprehensive integration of single-cell data. *Cell* 177, 1888–1902.e21. <https://doi.org/10.1016/j.cell.2019.05.031>.
- Subramanian, A., Sidhom, E.-H., Emani, M., Vernon, K., Sahakian, N., Zhou, Y., Kost-Alimova, M., Slyper, M., Waldman, J., Dionne, D., Nguyen, L.T., Weins, A., Marshall, J.L., Rosenblatt-Rosen, O., Regev, A., Greka, A., 2019. Single cell census of human kidney organoids shows reproducibility and diminished off-target cells after transplantation. *Nat. Commun.* 10, 5462. <https://doi.org/10.1038/s41467-019-13382-0>.
- Taguchi, A., Kaku, Y., Ohmori, T., Sharmin, S., Ogawa, M., Sasaki, H., Nishinakamura, R., 2014. Redefining the in vivo origin of metanephric nephron progenitors enables generation of complex kidney structures from pluripotent stem cells. *Cell Stem Cell* 14, 53–67. <https://doi.org/10.1016/j.stem.2013.11.010>.
- Taguchi, A., Nishinakamura, R., 2017. Higher-order kidney organogenesis from pluripotent stem cells. *Cell Stem Cell* 21, 730–746. <https://doi.org/10.1016/j.stem.2017.10.011>.
- Takasato, M., Er, P.X., Chiu, H.S., Maier, B., Baillie, G.J., Ferguson, C., Parton, R.G., Wolvetang, E.J., Roost, M.S., Chuva de Sousa Lopes, S.M., Little, M.H., 2015. Kidney organoids from human iPSCs contain multiple lineages and model human nephrogenesis. *Nature* 526, 564–568. <https://doi.org/10.1038/nature15695>.
- Tanigawa, S., Islam, M., Sharmin, S., Naganuma, H., Yoshimura, Y., Haque, F., Era, T., Nakazato, H., Nakanishi, K., Sakuma, T., Yamamoto, T., Kurihara, H., Taguchi, A., Nishinakamura, R., 2018. Organoids from nephrotic disease-derived iPSCs identify impaired NEPHRIN localization and slit diaphragm formation in kidney podocytes. *Stem Cell Reports* 11, 727–740. <https://doi.org/10.1016/j.stemcr.2018.08.003>.
- Tanigawa, S., Taguchi, A., Sharma, N., Perantoni, A.O., Nishinakamura, R., 2016. Selective in vitro propagation of nephron progenitors derived from embryos and pluripotent stem cells. *Cell Rep.* 15, 801–813. <https://doi.org/10.1016/j.celrep.2016.03.076>.
- van den Berg, C.W., Ritsma, L., Avramut, M.C., Wiersma, L.E., van den Berg, B.M., Leuning, D.G., Lievers, E., Koning, M., Vanslambrouck, J.M., Koster, A.J., Howden, S.E., Takasato, M., Little, M.H., Rabelink, T.J., 2018. Renal subcapsular transplantation of PSC-derived kidney organoids induces neo-vasculogenesis and significant glomerular and tubular maturation in vivo. *Stem Cell Reports* 10, 751–765. <https://doi.org/10.1016/j.stemcr.2018.01.041>.
- Volovelsky, O., Nguyen, T., Jarmas, A.E., Combes, A.N., Wilson, S.B., Little, M.H., Witte, D.P., Brunskill, E.W., Kopan, R., 2018. Hamartin regulates cessation of mouse nephrogenesis independently of Mtor. *Proc. Natl. Acad. Sci. Unit. States Am.* 115, 5998–6003. <https://doi.org/10.1073/pnas.1712955115>.
- Wang, F., Flanagan, J., Su, N., Wang, L.-C., Bui, S., Nielson, A., Wu, X., Vo, H.-T., Ma, X.-J., Luo, Y., 2012. RNAscope: a novel in situ RNA analysis platform for formalin-fixed, paraffin-embedded tissues. *J. Mol. Diagnostics* 14, 22–29. <https://doi.org/10.1016/j.jmoldx.2011.08.002>.
- Wang, P., Chen, Y., Yong, J., Cui, Y., Wang, R., Wen, L., Qiao, J., Tang, F., 2018. Dissecting the global dynamic molecular profiles of human fetal kidney development by single-cell RNA sequencing. *Cell Rep.* 24, 3554–3567.e3. <https://doi.org/10.1016/j.celrep.2018.08.056>.
- Wu, H., Uchimura, K., Donnelly, E.L., Kirit, Y., Morris, S.A., Humphreys, B.D., 2018. Comparative analysis and refinement of human PSC-derived kidney organoid differentiation with single-cell transcriptomics. *Cell Stem Cell* 23, 869–881.e8. <https://doi.org/10.1016/j.stem.2018.10.010>.
- Yokote, S., Matsunari, H., Iwai, S., Yamanaka, S., Uchikura, A., Fujimoto, E., Matsumoto, K., Nagashima, H., Kobayashi, E., Yokoo, T., 2015. Urine excretion strategy for stem cell-generated embryonic kidneys. *Proc. Natl. Acad. Sci. Unit. States Am.* 112, 12980–12985. <https://doi.org/10.1073/pnas.1507803112>.